Journal of Alloys and Compounds 509 (2011) 2273–2276

Contents lists available at ScienceDirect

Journal of Alloys and Compounds

journal homepage: www.elsevier.com/locate/jallcom

Novel hydroxyapatite–forsterite–bioglass nanocomposite coatings with improved mechanical properties

M. Mazrooei Sebdani*, M.H. Fathi

Biomaterials Group, Department of Materials Engineering, Isfahan University of Technology, Isfahan 84156-83111, Iran

ARTICLE INFO

Article history:
Received 23 August 2010
Received in revised form 11 October 2010
Accepted 28 October 2010
Available online 10 November 2010

Keywords:
Mechanical characterization
X-ray diffraction
Composites
Nanostructured materials

ABSTRACT

The purpose of this work was fabrication and evaluation of mechanical properties of hydroxyapatite–forsterite–bioactive glass nanocomposite coatings. The novel hydroxyapatite–forsterite–bioactive glass nanocomposite coating on 316L stainless steel (SS) was prepared via a sol–gel process. The X-ray diffraction (XRD), scanning electron microscopy (SEM), atomic force microscopy (AFM) and energy dispersive X-ray analysis (EDX) techniques were used to investigate the microstructure and morphology of the coatings. The local mechanical properties, e.g. nano-hardness, elastic modulus and fracture toughness of four type coatings with different amounts of forsterite, were determined by nano-indentation method using load and displacement data. The nano-indentation tester was equipped with Atomic Force Microscopy to image the indenter mark. The crack-free and homogeneous nanocomposite coatings with no observable defects were prepared. The coatings showed the hardness and elastic modulus values in the range of 2.4–3.4 (GPa) and 46–96 (GPa), respectively. The fracture toughness values of nanocomposite coatings also varied in the range of 0.56–0.972 (MPa $m^{0.5}$). The results showed that the elastic modulus, hardness and fracture toughness values of prepared composite coatings increased with increase in forsterite amounts. Results suggested that novel composite coatings might be potentially useful for biomedical applications especially as an implant coating for hard tissue treatment.

1. Introduction

Since calcium phosphates were identified, they have long been utilized for biomedical applications. Among which, a great deal of research has been focused on hydroxyapatite owing to its chemical and structural analogy to bone and teeth [1,2]. The usage of hydroxyapatite has been studied in the form of powders [3], coatings [4] or composites [5,6]. However, the poor mechanical properties such as the inherent brittleness, poor fatigue resistance and strength are the major limitation associated with the use of hydroxyapatite at high load bearing conditions [3]. As pointed out, hydroxyapatite has been mainly used as a porous coating on metallic implants in orthopedic and dental applications to combine the excellent mechanical properties of metals and bioactivity of hydroxyapatite, simultaneously [7–9]. On the other hand, composite coatings could be a subject of interest in order to achieve a combine of properties and overcome the main limitation of hydroxyapatite [10]. So, researches have been focused on adding other ceramics to hydroxyapatite coating [11]. One of the ceramic additions could be bioactive glasses. Along with hydroxyapatite, bioactive glasses within the $CaO–SiO_2–P_2O_5$ system could potentially be used as an additive due to considerable bioactivity performance [12]. In spite of improvement in bioactivity performance, it is observed that glass addition to hydroxyapatite coating decreases or does not affect on the mechanical properties of composite coatings [13–15]. To tackle this problem, it is needed to add other ceramics with better mechanical properties to hydroxyapatite–bioactive glass composite coatings. Forsterite could be a material of interest because of the superior mechanical properties than hydroxyapatite and bioactive glass. For instance, results showed that forsterite ceramics yield higher value in fracture toughness in comparison with hydroxyapatite and bioactive glass [16–18]. Moreover, it is expected that addition of these ceramics with reduced grain size lower than 100 nm improves the properties of the composite coatings [19]. In this case, Kharaziha and Fathi [16] showed that the dissolution rate of the forsterite nanopowder is higher than that of conventional forsterite powders and the stimulation for apatite formation is greater. So, it is expected that hydroxyapatite–forsterite–bioactive glass nanocomposite coatings have better bioactivity and mechanical properties than single hydroxyapatite and hydroxyapatite–bioactive glass nanocomposite coatings.

As the coated biomedical implants interact with the body environment, there is a need to directly evaluate the mechanical

* Corresponding author. Tel.: +98 311 3912750; fax: +98 311 3912752.
E-mail address: m.mazrooei@ma.iut.ac.ir (M.M. Sebdani).

0925-8388/$ – see front matter © 2010 Elsevier B.V. All rights reserved.
doi:10.1016/j.jallcom.2010.10.202

properties of the coated implant surface. Nano-indentation is an important tool to reveal the mechanical properties of thin films, coatings and composite materials [20].

The aim of this work was fabrication of novel hydroxyapatite–forsterite–bioactive glass nanocomposite coating via a sol–gel method and evaluation of mechanical properties of prepared composite coatings with different amounts of forsterite.

2. Materials and methods

2.1. Preparation and characterization of coating samples

The phosphoric pentoxide (P_2O_5, Merck), nitrate calcium tetrahydrate ($Ca(NO_3)_2{\cdot}4H_2O$, Merck), ethanol (Merck, 99.9%purity), forsterite nanopowder (Mg_2SiO_4, nano-sized (30–50 nm) spherical morphology) [16] and 45S bioactive glass nanopowder (nanoscale particles) [21] were used for preparing a sol which contains hydroxyapatite, forsterite and bioactive glass; 20 mm × 10 mm × 2 mm of stainless steel plates (SS316L) were selected as a substrate and polished to grade #1200 and then cleaned in an ultrasonic bath. Hydroxyapatite–forsterite–bioactive glass composite coatings were prepared by dipping substrates in a sol containing hydroxyapatite as a matrix with 10 wt% total amount of bioactive glass nanopowder and different amounts of forsterite nanopowders (0 wt % named F0, 10 wt % named F1, 20 wt % named F2, 30 wt % named F3) as reinforcements and withdrawing at a rate of 5 cm/min. After holding at ambient temperature for 24 h, samples were placed in an oven and dried at 80 °C for 24 h and then, were heat treated at 600 °C with 1 °C/min. The composite coatings with different amounts of forsterite were subjected to X-ray diffraction (XRD, Philips X'Pert-MPD) technique using a CuKα radiation generated at 40 kV and 30 mA in order to determine the phase composition. The Scherer's equation (Eq. (1)) was considered in order to calculate the apparent crystallite size of prepared composite coatings [22].

$$t = \frac{0.89\lambda}{\beta \cos\theta} \quad (1)$$

where β is the broadening of diffraction line measured at half its maximum intensity, λ is the wavelength (=0.154 nm), θ is the Bragg angle and t is the apparent crystallite size.

The surface of prepared coatings was observed using scanning electron microscopy (SEM, Phillips XL30). Atomic force microscopy (AFM) was used to characterize the topography of composite coating. Energy dispersive X-ray analysis (EDX, Seron AIS-2100) technique was used to determine the composition of the prepared composite coatings.

2.2. Mechanical property evaluations

The local mechanical properties of the composite coatings, e.g. nano-hardness and elastic modulus, were measured by the nano-indentation technique. Nano-hardness testing (NHT Compact platform, NHT-epx, CSM) (with a Berkovich tip) was suited to load and penetration depth measurements at nanometer length scales. The maximum of load and depth were 500 mN and 200 μm, respectively. The resolution of load and depth were 0.04 mN and 0.04 nm, respectively. The benefit of using nano-indentation technique is that the common approach for isolating the film properties of the substrate by making measurements to a maximum penetration depth of no more than 10% of the typical coating thickness. The nano-hardness (H) and elastic modulus (E) values were measured by the load–displacement plot using Oliver and Pharr (O-P) model [23]. The resulting load–displacement curves provided data specific to the mechanical nature of the material under examination. Established model was used to calculate quantitative hardness and elastic modulus values for such data. To reduce random errors, five different locations of each sample were tested.

On the other hand, the nano-indentation tester was equipped with AFM. A full AFM module (CSM-Bruker, Software siscanpanel 1.1) was used to provide a very quick way to image the residual indentation and associated cracks made by indenter with ultra high resolution [23]. Image-Pro Plus image measurement software was used to measure the crack length in order to calculate the fracture toughness. There are different equations introduced to measure the toughness of ceramic films and coatings so far [24]. In the present work, the following equation (Eq. (2)) was used to calculate the fracture toughness [23,25,26]:

$$K_{IC} = a^* \left(\frac{E_{IT}}{H_{IT}}\right)^{1/2} \left(\frac{F}{c^*}^{3/2}\right) \quad (2)$$

In the equation, K_{IC} is the fracture toughness, E_{IT} and H_{IT} are the instrumented elastic modulus and hardness, respectively, F is the applied load, c^* is the length of the radial cracks since the center of the indent, and a^* is an empirical constant that was taken as 0.016 for a Berkovich tip [26].

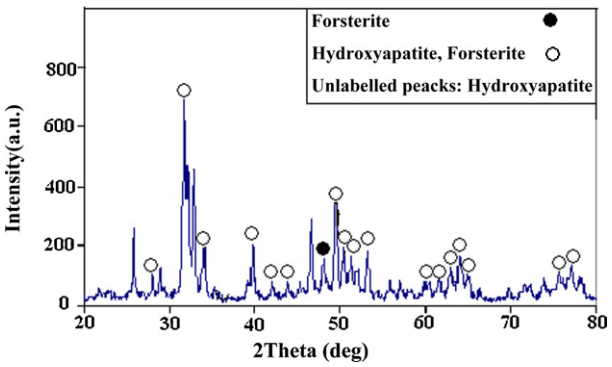

Fig. 1. X-ray diffraction pattern of prepared composite coating with 10 wt% of forsterite.

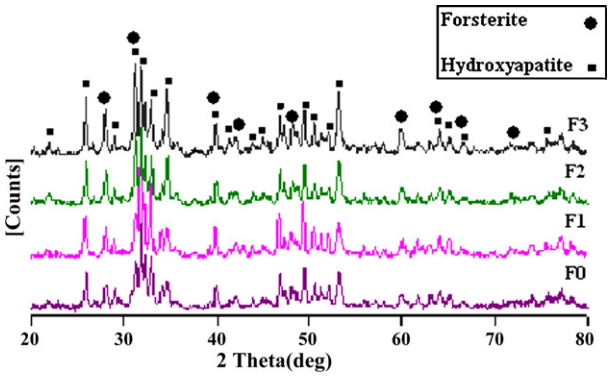

Fig. 2. X-ray diffraction patterns of prepared composite coatings. F0, without forsterite; F1, with 10 wt% forsterite; F2, with 20 wt% forsterite; F3, with 30 wt% forsterite.

3. Results and discussion

3.1. XRD analysis

Fig. 1 shows an XRD pattern of prepared composite coating with 10 wt% of forsterite. The XRD of composite coating showed the presence of hydroxyapatite and forsterite peaks in accordance with No: 09-0432 and No: 34-0189 files, confirming it to be free of additional crystalline phases such as CaO and β-TCP [3]. As clearly observed, constituent phases were stable. Therefore, no dissolution was observed at this temperature. This is in agreement with previous researches [18,27]. Fig. 2 shows XRD patterns of composite coatings with different amounts of forsterite. The crystallite size of hydroxyapatite in prepared composite coatings determined by using Eq. (1) was lower than 100 nm (about 30–50 nm).

3.2. SEM and AFM evaluations and EDX analysis

Fig. 3 shows the SEM micrograph of hydroxyapatite–forsterite–bioactive glass composite coating with 10 wt% of forsterite. The crack-free and homogeneous hydroxyapatite–forsterite–bioactive glass composite coating was observed with no observable defects. The thickness of prepared composite coatings with different amounts of forsterite was about 20–30 μm.

Fig. 4 shows a typical 3D AFM topography of a composite coating. The AFM image shows that flat surface was rough. The particle sizes determined with AFM were lower than 100 nm.

The EDX spectra of hydroxyapatite–forsterite–bioglass coated 316L SS surface is shown in Fig. 5. The peaks of O, Si, P and Ca belong to the consisting elements of prepared coating and the peaks of Fe, Cr and Ni belong to 316 L SS.

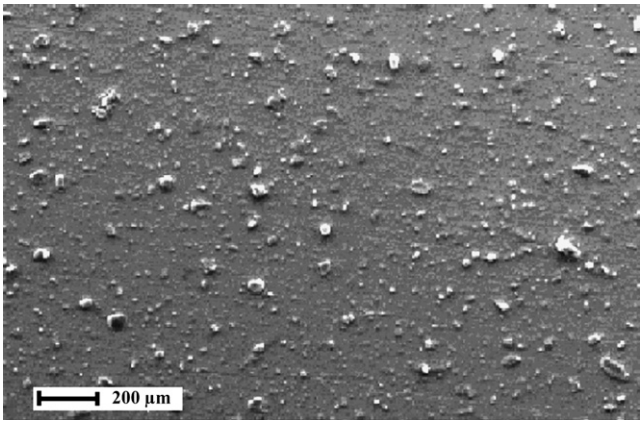

Fig. 3. SEM micrograph of hydroxyapatite–forsterite–bioglass composite coating with 10 wt% of forsterite.

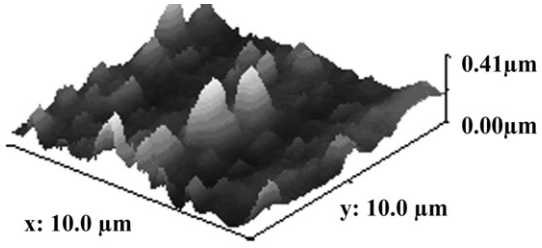

Fig. 4. 3D typical AFM topography of prepared composite coatings.

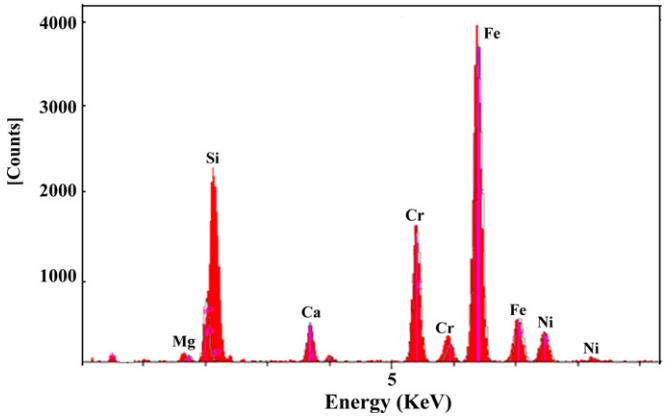

Fig. 5. Energy dispersive X-ray analysis (EDX) of the hydroxyapatite–forsterite–bioactive glass coated 316L SS sample.

3.3. Nano-hardness, elastic modulus and fracture toughness

Fig. 6 shows the obtained load–displacement curves of prepared coatings with different amounts of forsterite at a load of 30 mN. The differences in the depth obtained at the applied load represent the differences in hardness of the materials. As clearly observed, with increasing forsterite content in the composite coating, the penetration depth of the indenter decreased. As a result, among all the composite coatings, a composite coating with the most amount of forsterite was the hardest coating and the composite coating without forsterite was the softest coating dealt in the present investigation. The measured values of hardness are in agreement with similar values reported by other researchers for hydroxyapatite coatings [28–31]. The hardness value of hydroxyapatite coatings that were prepared via radio frequency magnetron and pulsed laser deposition were in the range of 2.5–3 GPa and 4.5–5.2 GPa, respectively [29,30]. Dey et al. [31] reported the hardness value of hydroxyapatite coatings in the range of 1.5–5 GPa. Fig. 7 shows a typical AFM image of the indent marks for composite coatings. As shown, the indentation area seemed smooth without any impending sign of severe damage growth or accumulation. Table 1 gives the elastic modulus and hardness values of composite coating with different amounts of forsterite. The fracture toughness values calculated based on Eq. (2) were also given in Table 1. The fracture toughness values of prepared composite coatings with different

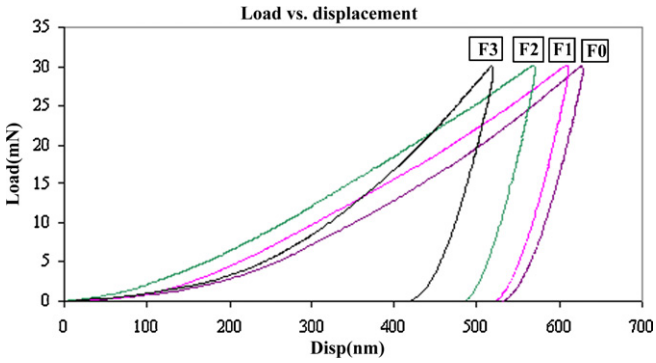

Fig. 6. The load-depth plots of four types of composite coatings with different amounts of forsterite. F0, without forsterite; F1, with 10 wt% forsterite; F2, with 20 wt% forsterite; F3, with 30 wt% forsterite.

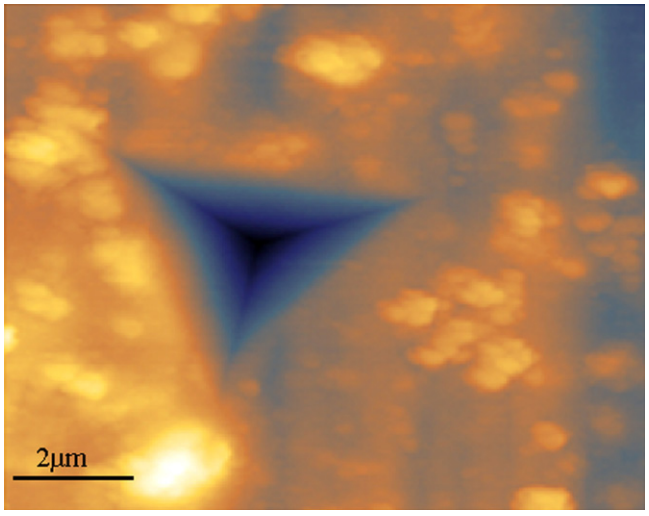

Fig. 7. Typical AFM image of the indent marks for prepared composite coatings.

Table 1
Modulus, hardness and fracture toughness values of prepared composite coatings.

	Hardness (MPa)	Elastic modulus (GPa)	Fracture toughness (MPa $m^{1/2}$)	Load (mN)
F0	2384	46	0.56	30
F1	2812	70	0.688	30
F2	3293	85	0.75	30
F3	3388	96	0.972	30

Composite coating: F0, without forsterite; F1, with 10 wt% forsterite; F2, with 20 wt% forsterite; F3, with 30 wt% forsterite.

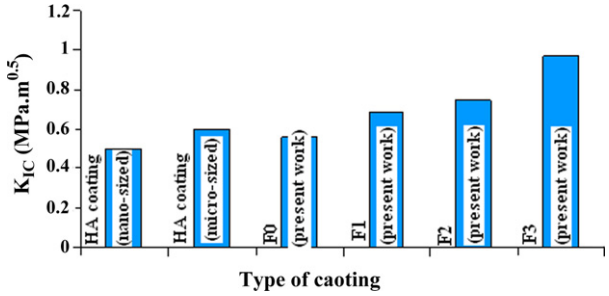

Fig. 8. Comparison of fracture toughness of hydroxyapatite (HA) with different sizes from literature data and hydroxyapatite-included composite coating from present work. F0, without forsterite; F1, with 10 wt% forsterite; F2, with 20 wt% forsterite; F3, with 30 wt% forsterite.

amounts of forsterite were in the range of 0.56–0.972 MPa m$^{0.5}$. The composite coatings in the present study show higher values of fracture toughness than the reported values for hydroxyapatite coatings: 0.45 MPa m$^{0.5}$ by Wang et al. [32] for hydroxyapatite coatings prepared via macroplasma spraying process, 0.5 MPa m$^{0.5}$ by Li et al. [33], for hydroxyapatite coatings prepared via high velocity oxy fuel technique, 0.6 MPa m$^{0.5}$ by Dey and Mukhopadhyay [34], for hydroxyapatite coatings prepared via microplasma spraying process, 0.6 MPa m$^{0.5}$ by Ben-Nissan for sol–gel derived nanoscale hydroxyapatite coatings [35]. It could be attributed to nano-sized constituent phases and a high elastic modulus of prepared composite coatings. Fracture toughness of coatings increases as the particle size of constituent phases decreases [32]. Fig. 8 shows the comparison of fracture toughness of hydroxyapatite with different sizes from literature data and composite coatings from present work. As shown, the presence of nano-sized reinforcements is an important factor for enhancing fracture toughness. This effect was similar to that reported for other reinforcements introduced to hydroxyapatite coatings. There have been several attempts to enhance the fracture toughness of hydroxyapatite coating by introducing of a second phase, for example fluorine [36], yttria-stabilized zirconia [37], titanium dioxide [38] and carbon nanotube [39]. Zhang et al. [36] have reported 0.12–0.31 MPa m$^{0.5}$ for the value of fracture toughness of fluoridated hydroxyapatite coatings. Fu et al. [37] have reported 0.8436–1.09 MPa m$^{0.5}$ for the value of fracture toughness of yttria-stabilized zirconia reinforced hydroxyapatite coatings. Li et al. [38] have reported 0.48–0.67 MPa m$^{0.5}$ for the value of fracture toughness of titanium dioxide reinforced hydroxyapatite coatings. The obtained results confirmed the influence of forsterite nanopowder amounts on the mechanical properties of hydroxyapatite–forsterite–bioactive glass nanocomposite coatings. But a more direct and strict comparison of the data of the present work with literature data was not possible because the reported data obtained from different conditions.

4. Conclusions

Novel hydroxyapatite–forsterite–bioactive glass composite coatings were successfully prepared by a sol–gel method. The crack-free and homogeneous nanocomposite coatings were obtained with no observable defects. The hardness and elastic modulus values of prepared coatings were obtained in the range of 2.4–3.4 (GPa) and 46–96 (GPa), respectively, regarding the increase in the amounts of forsterite. The fracture toughness values of prepared composite coatings varied in the range of 0.56–0.972 (MPa m$^{0.5}$). Results indicated that improvement of the mechanical properties could be obtained with increase in forsterite amounts, and suggest that composite coatings might be good candidates for biomedical applications such as human body implant coatings for hard tissue treatment.

Acknowledgements

The authors thank for support of this research by Isfahan University of Technology.

References

[1] F.H. Albee, H.F. Morrison, Ann. Surg. 71 (1920) 32.
[2] L.L. Hench, J. Am. Ceram. Soc. 74 (1991) 1487.
[3] M.H. Fathi, A. Hanifi, Mater. Lett. 61 (2007) 3978–3983.
[4] Y. Sung, J. Lee, J. Yang, J. Cryst. Growth 262 (2004) 467.
[5] A. Balamurugan, G. Ballosier, S. Kannan, S. Rajeswari, Mater. Lett. 60 (2006) 2288–2293.
[6] Y. Sung, D. Kim, J. Cryst. Growth 254 (2003) 411.
[7] H. Kusakabe, T. Sakamaki, K. Nihei, Y. Oyama, S. Yanagimoto, M. Ichimiya, Biomaterials 25 (2004) 2957.
[8] J.L. Ong, D.C.N. Chan, Annu. Rev. Biomed. Eng. A 28 (2000) 667.
[9] K.A. Gross, C.S. Chai, G.S.K. Kannangara, B. Ben-Nissan, J. Mater. Sci.: Mater. Med. 9 (1998) 839–843.
[10] M.H. Fathi, M. Salehi, A. Saatchi, V. Mortazavi, S.B. Mousavi, Dent. Mater. 19 (2003) 188.
[11] S.J. Ding, Y.M. Su, C.P. Ju, J.H. Chern Lin, Biomaterials 22 (2001) 833–845.
[12] A. Balamurugan, G. Sockalingum, J. Michel, J. Faure, V. Banchet, L. Wortham, Mater. Lett. 60 (2006) 3752–3757.
[13] N. Li, Q. Jie, S. Zhu, R. Wang, Mater. Lett. 58 (2004) 2747–2750.
[14] F.N. Oktar, G. Guller, Ceram. Int. 28 (2002) 617–621.
[15] S.J. Ding, C.P. Ju, J.H. Chern Lin, Mater. Sci.: Mater. Med. 11 (2000) 183–190.
[16] M. Kharaziha, M.H. Fathi, Ceram. Int. 35 (2009) 2449–2454.
[17] M.H. Fathi, M. Kharaziha, J. Alloys Compd. 472 (2009) 540–545.
[18] M.H. Fathi, M. Kharaziha, Mater. Lett. 63 (2009) 1455–1458.
[19] G. Chen, G.X. Sun, Z.G. Zhu, Mater. Sci. Eng. A 265 (1999) 197.
[20] S. Saber Samandari, K.A. Gross, Surf. Coat. Technol. 203 (2009) 3516–3520.
[21] M.H. Fathi, Doost mohammadiF A., Mater. Sci. Eng. A. 474 (2008) 128–133.
[22] B.D. Cullity, Elemeny of XRD diffraction, Addison-Wesley, 1978.
[23] W.C. Oliver, G.M. Pharr, J. Mater. Res. 7 (1992) 1564–1583.
[24] S. Zhang, D. Sun, Y.Q. Fu, H. Du, Surf. Coat. Technol. 198 (2005) 74.
[25] A.G. Evans, B.R. Lawn, D.B. Marshall, J. Am. Ceram. Soc. 63 (1980) 574–581.
[26] S. Zhang, D. Sun, Y. Fu, H. Du, Surf. Coat. Technol. 198 (2005) 74–84.
[27] J.M. Gomez-Vega, E. Saiz, A.P. Tomsia, M. Goldman, G.W. Marshall, S.J. Marshall, Biomaterials 23 (2002) 3749–3756.
[28] R. Roop Kumar, M. Wang, Mater. Sci. Eng. A 338 (2002) 230–236.
[29] V. Nelea, C. Morosanu, M. Iliescu, I.N. Mihailescu, Appl. Surf. Sci. 228 (2004) 346–356.
[30] V. Nelea, C. Morosanu, M. Iliescu, I.N. Mihailescu, Surf. Coat. Technol. 173 (2003) 315–322.
[31] A. Dey, A.K. Mukhopadhyay, S. Gangadharan, M.K. Sinha, D. Basu, N.R. Bandyopadhyay, Ceram. Int. 35 (2009) 2295–2304.
[32] M. Wang, X.Y. Yang, K.A. Khor, Y. Wang, Mater. Sci.: Mater. Med. 10 (1999) 269–273.
[33] H. Li, K.A. Khor, P. Cheang, Surf. Technol. Coat. 155 (2002) 21–32.
[34] A. Dey, A.K. Mukhopadhyay, Int. J. Appl. Ceram. Technol. (2010).
[35] R. Roest, G. Heness, B.A. Lattela, B. Ben-Nissan, Key. Mater. Eng. 306–308 (2006) 1307–1312.
[36] S. Zhang, Y.S. Wang, X.T. Zeng, K.A. Khor, W. Weng, D.E. Sun, Thin Solid Films 516 (2008) 5162–5167.
[37] L. Fu, K.A. Khor, J.P. Lim, Mater. Sci. Eng. A 316 (2001) 46–51.
[38] H. Li, K.A. Khor, P. Cheang, Biomaterials 23 (2002) 85–91.
[39] K. Balani, R. Anderson, T. Laha, M. Andara, Biomaterials 28 (2007) 618–624.